Novel fracture zone identifier attribute using geophysical and well log data for unconventional reservoirs

Debotyam Maity[1] and Fred Aminzadeh[2]

Abstract

We have characterized a promising geothermal prospect using an integrated approach involving microseismic monitoring data, well logs, and 3D surface seismic data. We have used seismic as well as microseismic data along with well logs to better predict the reservoir properties to try and analyze the reservoir for improved mapping of natural and induced fractures. We used microseismic-derived velocity models for geomechanical modeling and combined these geomechanical attributes with seismic and log-derived attributes for improved fracture characterization of an unconventional reservoir. We have developed a workflow to integrate these data to generate rock property estimates and identification of fracture zones within the reservoir. Specifically, we introduce a new "meta-attribute" that we call the *hybrid-fracture zone-identifier attribute* (FZI). The FZI makes use of elastic properties derived from microseismic as well as log-derived properties within an artificial neural network framework. Temporal analysis of microseismic data can help us understand the changes in the elastic properties with reservoir development. We demonstrate the value of using passive seismic data as a fracture zone identification tool despite issues with data quality.

Introduction

Passive seismic as a tool for monitoring reservoirs has become fairly routine in recent years. Two of the more common applications include development of unconventional reservoirs such as geothermal systems, tight gas fields, or oil reservoirs that require fluid injection, monitoring of CO_2 injection, and water and steam flooding. The use of conventional seismic data for reservoir characterization is a fairly well understood area of study with multiattribute analysis. Seismic attributes are evaluated based on observed changes in the seismic signal because of various underlying physical phenomenon. Elastic wave propagation through the subsurface is influenced by structural as well as stratigraphic features. Attributes provide specific geometric, kinematic, geomechanical, dynamic, or structural measures of these features. Conventional seismic attribute analysis includes amplitude (for lithological contrasts, fluid content, and gross porosity), instantaneous frequency (for bed thickness, fluid content, and fractured zones), coherency (to highlight discontinuities), envelope (for bright spots, thin beds, and lateral discontinuities), and impedance (for porosity, unconformities, and elastic properties) to name a few. All of these attributes, as well as many others, are extensively used today for various reservoir characterization schemes (Taner et al., 1979; Chopra and Marfurt, 2007b).

The concept of combining seismic attributes to detect specific seismic anomalies by clustering analysis was introduced by Aminzadeh and Chatterjee (1984). Many other work to combine attributes through regression analysis, fuzzy clustering, self-organizing networks, and weighted attributes, as well as through other means are introduced by Russel et al. (1997), Schuelke et al. (1998), Lashgari (1991), Walls et al. (1999), Barnes (2000), and Chopra and Marfurt (2007a).

A new class of attributes, referred to as *meta-attributes*, is introduced by Aminzadeh (2003, 2005). Meta-attributes (or hybrid attributes because we are using the terminologies interchangeably) not only aggregate different attributes but also combine the artificial intelligence of an artificial neural network (ANN) with the human intelligence of an interpreter (who provides input to the training process of the ANN) to create an attribute fit for a purpose. As described in Aminzadeh (2003), we are looking at a set of computer algorithms that are developed to search through data volumes looking for specific types of anomalous sections in the seismic data using carefully designed criteria or "meta-attributes." Meta-attributes are an aggregation of several seismic attributes combined with the interpreter's insight through a neural network to detect a particular feature. A typical example would be Aminzadeh and Connolly (2002) in which the gas chimney is

[1]Gas Technology Institute, Des Plaines, Illinois, USA. E-mail: debotyam.maity@gastechnology.org.
[2]University of Southern California, Los Angeles, California, USA. E-mail: faminzad@usc.edu.

Manuscript received by the Editor 6 January 2015; revised manuscript received 20 April 2015; published online 25 June 2015. This paper appears in *Interpretation*, Vol. 3, No. 3 (August 2015); p. T155–T167, 18 FIGS.
http://dx.doi.org/10.1190/INT-2015-0003.1.

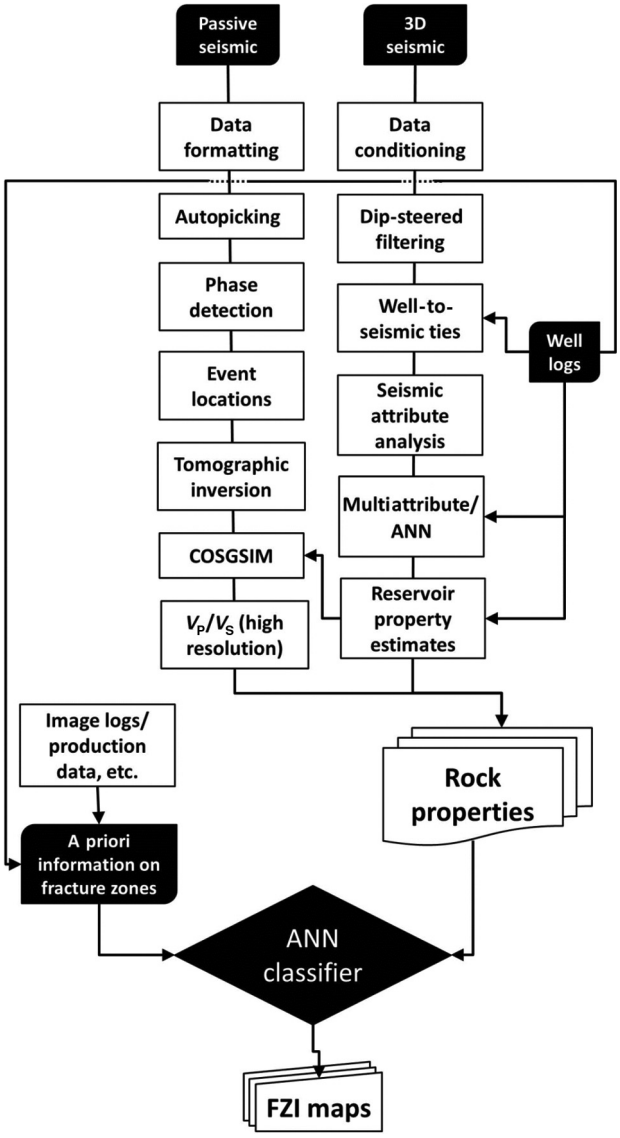

Figure 1. Integrated workflow for reservoir characterization — outline.

the intended meta-attribute. Aminzadeh et al. (2005) use the meta-attribute concept to derive the hydrocarbon probability index from the AVO data. Likewise, Aminzadeh and Brouwer (2006) extend the meta-attribute concept to introduce a hybrid neurofuzzy workflow for prospect identification and ranking by manipulating traditional seismic attributes.

Other recent studies have shown ways of combining conventional seismic attributes with geometric and geomechanical attributes to characterize unconventional shale environments (Trinchero et al., 2013). Attribute integration methods can range from simple corendering techniques (Gupta et al., 2011) to complex neural networks-based property modeling approaches (Clifford and Aminzadeh, 2011). Although conventional seismic data acquisition is fairly common for reasonably big reservoirs including large shale plays, they are seldom acquired in small unconventional reservoir settings. Moreover, the use of passive seismic monitoring is primarily focused on understanding the fracturing process and is underutilized as a tool for reservoir property prediction. In this study, we have used seismic as well as microseismic data along with well logs to better predict the reservoir properties to try and analyze the reservoir for improved mapping of natural and induced fractures open to flow. We use microseismic derived velocity models for geomechanical modeling and combine these geomechanical attributes with seismic and log-derived attributes for improved fracture characterization of an unconventional reservoir. Figure 1 shows a basic workflow outlining the various parts of the integrated analysis scheme to provide an overview of the techniques used.

We have applied the meta-attribute concept to a complex geothermal field within a fluvial setting in a region showing intense geologic activity. Our approach involves simultaneous use of microseismic data, 3D seismic data, and well logs. This is followed by integrated data analysis and characterization methods with shared results including fracture zone identification. Finally, discontinuity and fractured zone mapping-based interpretations are used to demonstrate their value in understanding the reservoir behavior and optimizing overall productivity. Maity (2013) provides for a more complete understanding of the data used and our approach.

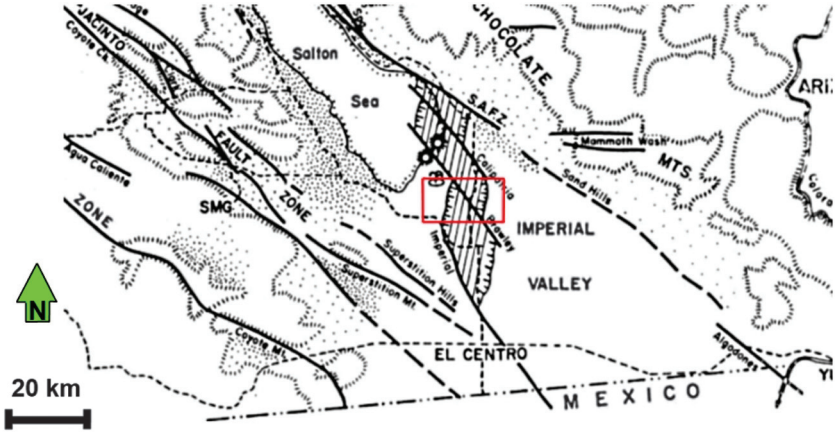

Figure 2. Fault map showing the Salton Trough as well as the study area in question. The patterned lines show the spreading centers. SMG, Split Mountain Gorge (modified from Crowell and Sylvester, 1979).

Geologic setting

The geothermal field in question is located in the Imperial Valley of Southern California, which is a part of the Salton Trough. The Salton Trough belongs to the Gulf of California segment of the Eastern Pacific Rise and forms a transition between the San Andreas Fault system to the east and spreading ridge complex to the northwest. Over millions

of years, the Colorado River has carried and deposited sediments into the system creating the current sedimentary geologic setting. Figure 2 shows the setting in some detail, highlighting the major fault systems at play close to the study area as well as the spreading zone.

The deltaic sedimentary sequence consists of alternating sand, silts, and clays, which extend beyond a depth of 15,000 ft. At shallower depths, the sediments encountered are primarily nonmarine sands and clays that are highly unconsolidated. The deeper formation is composed of marine deposits of sandstones and mudstones, which become more consolidated with depth because of compaction and cementation with carbonates and silica. Very low matrix permeability is observed at deeper intervals, and the corresponding temperature profiles suggest that permeability is related to pore-space cementation by fluid circulation. The focus of this investigation is the shallower reservoir above 5000 ft where the reservoir porosities and permeabilities are substantially higher. The resource in question is a hydrothermal system (no in situ or produced steam) with temperatures in the reservoir ranging from 300°F to 400°F and brines of moderate salinity (up to 40,000 ppm). The sands encountered in the reservoir are very fine grained, well sorted, and relatively clean. However, one of the major unanswered questions is that of continuity of the shallower sands (which is a result of active geologic and deltaic environment). We also know that the reservoir is highly fractured (Matlick and Jayne, 2008) and their distribution is the key in understanding productivity behavior and injectivity issues. This has led to a highly challenging play with major unresolved issues such as abnormal pressure decline and flow throughput issues (P. Walsh, personal communication, 2012). The primary objective of this study is to validate the potential use of the newly defined hybrid attribute in characterizing the observed reservoir behavior.

3D seismic data analysis

A 3D surface seismic survey consisting of 31 north–south receiver lines and 12 east–west source lines with east–west orientation was acquired over the target in 2010. The sweep frequency range used was from 4 to 88 Hz, and the sweep length was 8 s (Figure 3). The 3D seismic data are used to identify major discontinuity features and other estimates including log-derived property volumes for our analysis. Acoustic impedance is used as a secondary constraint for improving the resolution of the V_P and V_S models using the sequential Gaussian cosimulation algorithm as discussed in the next section. Figure 4 shows the seismic cross section and discontinuity attribute at referenced inline and crossline locations. The small range of seismic survey limits the comprehensive illumination of the subsurface environment. The observed discontinuity over the entire survey is caused by loosely bound alluvial sediments. This unconsolidation leads to reduced spatial continuity making the process of picking horizons highly challenging.

Well logs are used to obtain seismic to well ties to do a preliminary time-to-depth conversion after undertaking the initial data processing and conditioning. Two wells with available sonic logs are used to obtain a generalized power law relationship between traveltime and resistivity (similar to Faust, 1953) in which the constants are computed through regression analysis of the available log data. This relation is in turn used within other wells to obtain pseudo-sonic logs (Rudman et al., 1976). Figure 5 shows a crossplot of actual and pseudo-sonic log for one of the two control wells with available log data for reference. The logs obtained are then combined with density data to generate impedance logs. The reflection coefficients obtained are then convolved with a selected seismic wavelet to obtain a synthetic seismic trace. The synthetic trace is compared with the actual seismic trace extracted from a volume around the corresponding well track, and major reflectors are matched to obtain acceptable ties for all available wells.

The depth-stretched seismic volume and logs are next used to predict reservoir log properties such as porosity and density using an ANN-based approach. Seismic attributes (Chopra and Marfurt, 2007a) are calculated from the seismic amplitude data and used as input in a supervised neural network framework, which attempts to predict the desired output property. The input parameters used for property prediction include inverted impedance, V_P/V_S ratio, bulk modulus, and Poisson's ratio. Figure 6 shows sample properties at reference depth (1 km) estimated using this methodology with superimposed well locations for reference. These properties are useful input to our fracture zone characterization

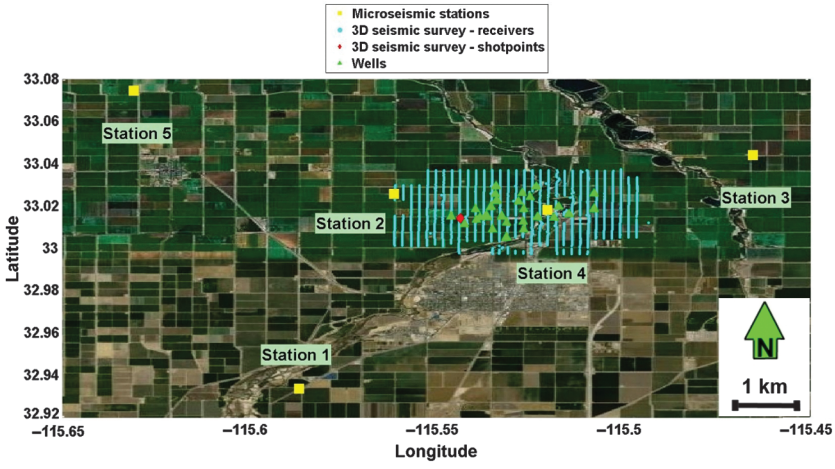

Figure 3. Integrated display of survey area with location of microseismic recording stations, wells and 3D seismic survey (receiver and shot locations).

framework and help in obtaining elastic properties using inverted wave velocities. We use colored inversion (Lancaster and Whitcombe, 2000) to convert seismic data to acoustic impedance. Pseudologs from properties estimated using ANN-based modeling are compared with actual logs to validate the property estimates before their use in characterization workflows. We use Laplacian (edge-enhancement methods based on dip steered second-order spatial derivatives [Jahne, 1993]) and amplitude variance (Bakker et al., 1999) to evaluate discontinuities as shown in Figure 6. These discontinuity maps are used to support interpretations made using the derived attributes to improve our understanding of reservoir behavior.

Passive seismic data analysis

A passive seismic array placed in shallow boreholes was used to continuously monitor the operations of the field since 2008. The data acquisition array for the data used in this study included five recording stations each recording 3C data as shown in Figure 3.

Microseismic data processing involves multiple steps starting with the use of a simple energy ratio-based triggering scheme to identify potential events in the passive seismic data sets by comparing with predefined normalized thresholds. The triggered data are appropriately time stamped and run through an advanced neural network-based autopicker (Maity et al., 2014). These picks are inverted for location and velocity. A double-difference algorithm (Waldhauser and Ellsworth, 2000) is used to obtain hypocentral locations based on the event arrival time differentials based on generated P- and S-wave arrival data as well as the initial local crustal model for the study area, which is sourced from Southern California Earthquake Data Center (SCEDC, 2013). Figure 7 shows the spatial distribution of the hypocenters as they relate to the injector/producer locations. Because of very few local passive seismic sensors, the ability to accurately resolve source parameters for most events was low with around 5% of the actual triggers being used for further analysis. Conse-

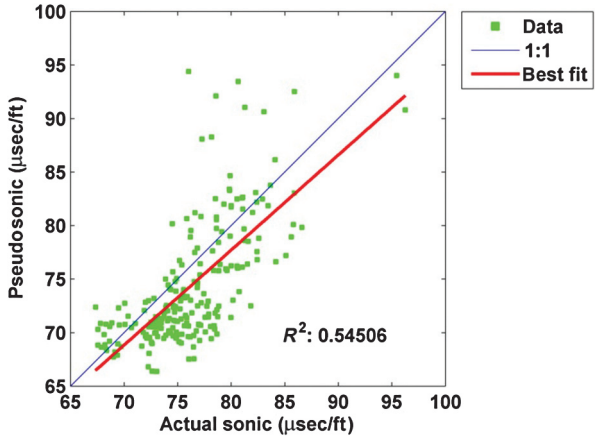

Figure 5. Crossplot of actual and resistivity derived pseudosonic log as obtained through regression analysis.

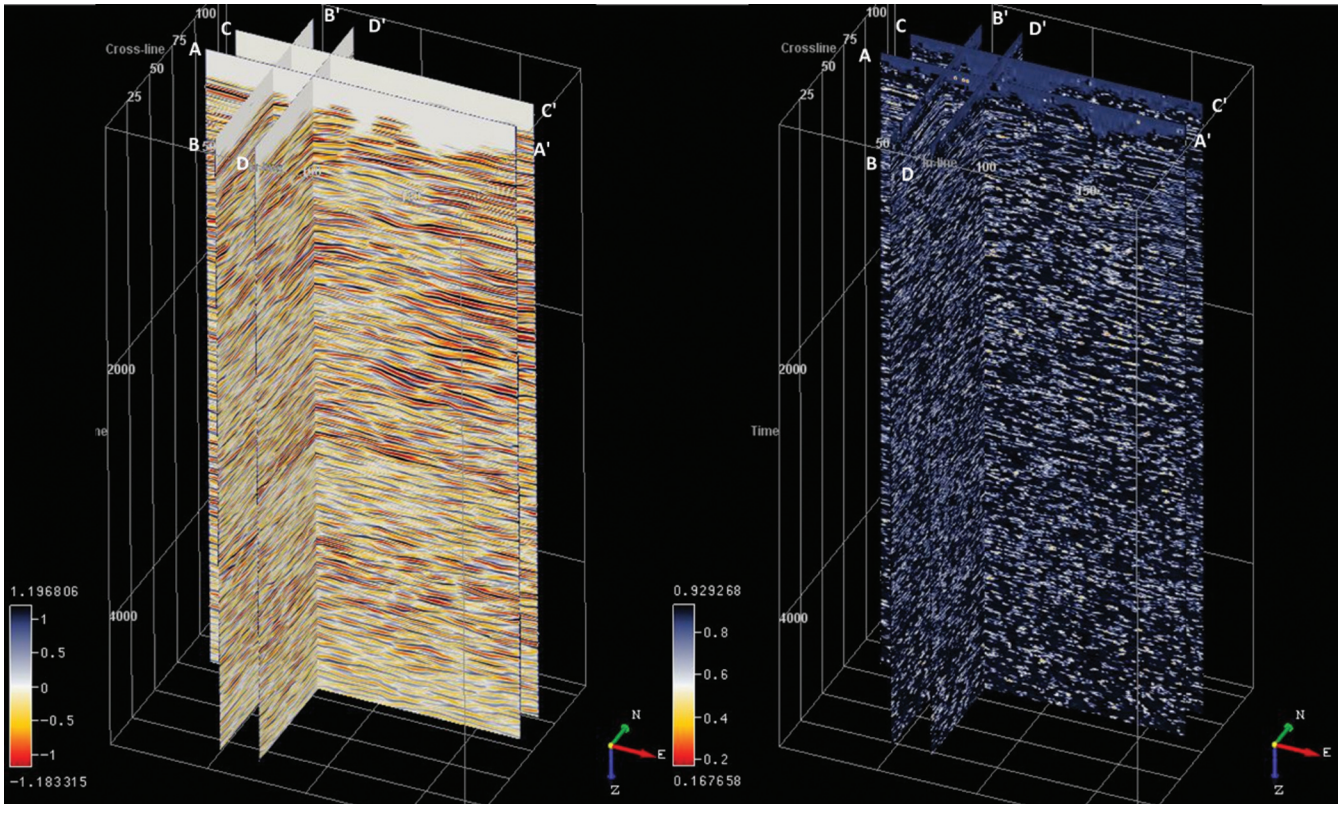

Figure 4. Time-migrated seismic amplitude as well as discontinuity attributes along vertical slices (AA′, BB′, CC′, and DD′).

quently, very few events within the actual study area could be adequately resolved. Furthermore, some of the larger events fall outside of the actual study volume. From the regional geologic setting, we know that there are some major faults extending southeast of study area, which could be causing the seismicity (either natural or triggered from water injection). Despite the limited use of the hypocenters in better understanding the interaction of fluid injection and the subsurface features, we look at the potential of using inverted velocities to better define the perturbed zone. The hypocenters obtained are used to generate improved velocity models by using simultaneous P- and S-inversion algorithms (Thurber, 1993). This algorithm uses the P- and S-wave information along with preliminary velocity model estimates and progressively iterates over all of the traveltime data available to provide final hypocentral and velocity estimates. The cell size used in tomography is approximately 15 times larger than the grid size for 3D seismic data. One of the guiding reasons behind lower resolution was the lack of adequate passive seismic data for accurate inversion/tomography workflows at high resolutions. With better data quality (resulting from more robust survey designs), the resolution and accuracy of the tomography results could be improved. Some elements of optimal survey design include reservoir controls such as structural/stratigraphic features, data quality/processing requirements, redundancy, noise, instrumentation, etc. The reader is encouraged to refer available literature (Curtis et al., 2004; Maity et al., 2013) on optimizing passive seismic surveys aimed at imaging local seismicity.

After adequate iterative runs involving the removal of bad phase arrival data and improving coverage by considering an adequate number of events based on known sensor array spread, the final velocity models are obtained and used as a baseline estimate for the area of interest. We then use Stanford Geostatistical

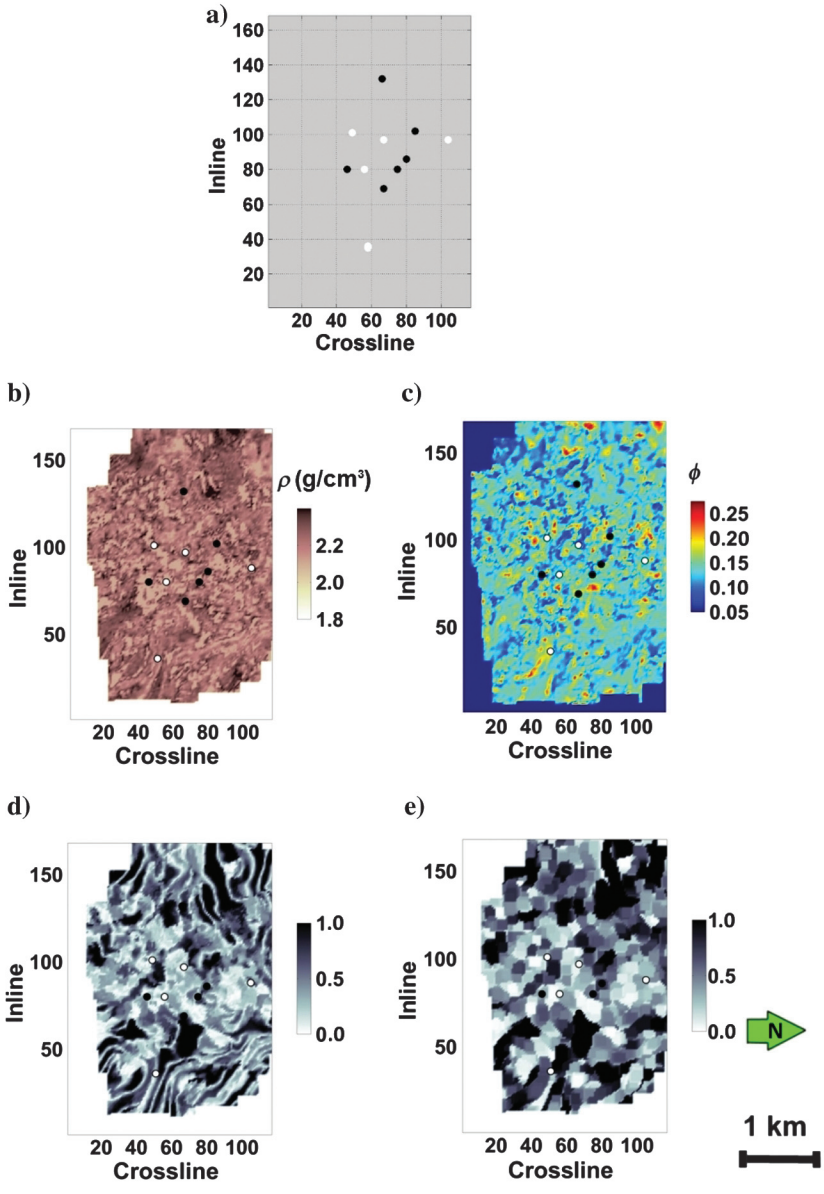

Figure 6. Depth slices at $Z = 1$ km through (b) density, (c) porosity, (d) edge-enhanced, and (e) edge-preserved seismic amplitude volumes. Panel (a) indicates well control (white, injectors; and black, producers).

Modeling Software (Remy et al., 2009) to populate the study area by using sequential Gaussian cosimulation algorithm involving seismic derived impedance as the secondary data to obtain high-resolution P- and S-wave velocity estimates. We validate the use of acoustic impedance by looking for correlations with phase velocities at multiple zones of interest. Enhancement in resolution of wave velocities is based on the simulation technique used and a relatively higher mismatch is expected because of the poor quality of passive seismic data available for this study. As highlighted earlier, with improved data quality, we should get improved tomographic resolution allowing for better property estimates. We calculate simulation uncertainty using statistical analysis of the final velocity realizations. This is done by generating 36 realizations and observing the standard deviations at each evaluation point. The final selection of V_P and V_S models is based on least-squares error evaluation using the sparse velocity field input at original locations for reference. The simulation uncertainty is combined with the uncertainty derived from the resolution of the velocity inversion result. The resolution of the model is computed using the resolution and covariance matrix computed with the SimulPS algorithm. Figure 8 shows representative V_P and V_S maps and associated estimation error at a reference depth of 1 km and Figure 9 shows the correlation obtained with VP at two separate depths (0.5 and 1.0 km) for reference.

The V_P and V_S can be related to elastic properties including bulk modulus, shear modulus, and Poisson's ratio, and these can be used to characterize zones of interest using available frameworks to relate the geophysical and geomechanical properties with reservoir attributes such as fractures (Toksöz and Johnston, 1981). Estimation of rock properties based on microseismic-derived wave velocity estimates has been demonstrated as a viable tool for reservoir characterization (Maity and Aminzadeh, 2012). We know that V_P and V_S can be used to derive Lamé's parameters (Mavko et al., 2003), which in turn are used to estimate the inertial properties of the rock (Beer et al., 2009). We can further calculate estimates of extensional and hydrostatic stress directly using V_P and V_S estimates obtained earlier (Toksöz and Johnston, 1981). Extensional stress tends to pull rocks apart, whereas hydrostatic stress is a confining stress that is compressive in nature.

There are several observations that can be made using these property estimates, particularly by combining with properties estimated using conventional seismic data. The applicability of traditional poroelastic theory in the field holds because of the sedimentary nature of the geothermal reservoir in question and relatively low temperatures involved because of the absence of steam. The closing of small fractures because of increasing pressure with depth or cementation effects should cause an increase in seismic velocity. Fracturing, chemical alteration, and extreme temperature gradients, etc., can cause a reduction in seismic velocities. Fluid saturation tends to reduce V_S and enhance V_P/V_S and Poisson's ratio. For highly fractured gas-saturated zones, we can generally expect low V_P and V_S values and reduced V_P/V_S velocity ratios. These and other effects such as the effect of fractures on porosities, acoustic impedance, bulk densities, etc., can be used in an integrated manner to identify fractured zones or other intervals of interest. Figure 10 shows sample distributions for some of these properties mapped at reference depth of 1.0 km.

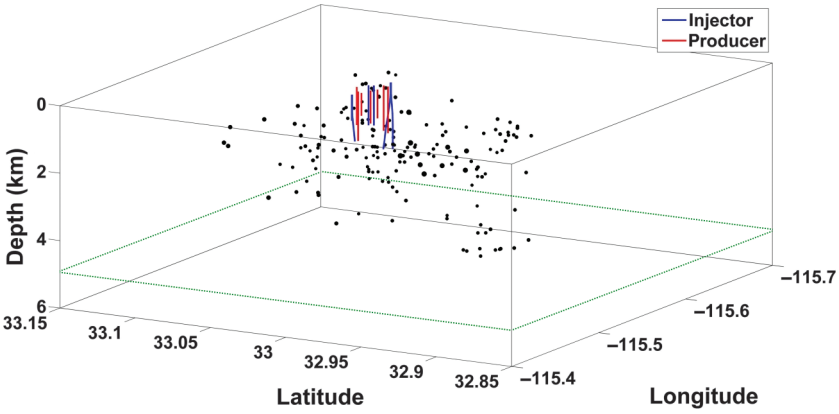

Figure 7. Event hypocenter distribution (size of dots represents the event magnitudes). We can clearly observe that most events fall outside the injection area indicating very high local seismicity near Salton Trough. The green inserts indicate approximate location of basement.

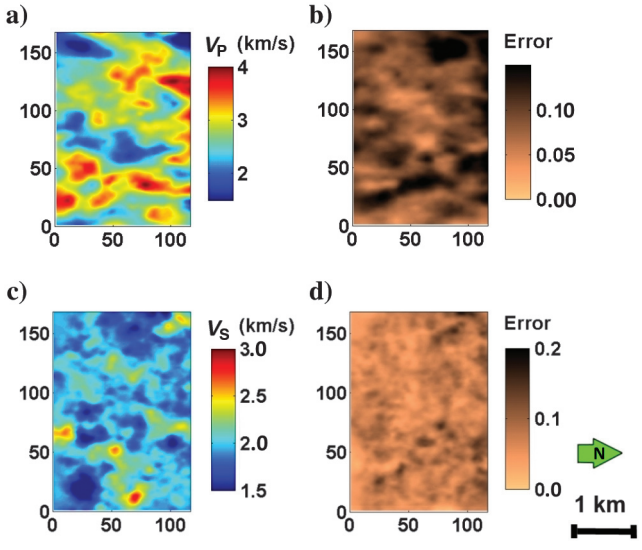

Figure 8. Depth slices at $Z = 1$ km through (a) V_P, (b) V_P simulation error, (c) V_S, and (d) V_S simulation error volumes.

Integrated reservoir characterization

The property estimates obtained from microseismic data analysis as well as those obtained from 3D seismic data using a neural network-based well log property prediction workflow can be combined based on the expected target zone observations such as high porosity, low density, and low impedance values. Moreover, elastic rock properties as well as stress observations can be used to interpret possible zones of fracturing. Low V_P/V_S anomalies and low V_P anomalies could potentially be fracture induced. Moreover, low extensional stress anomalies indicate open fracture zones (Berge et al., 2001; Martakis et al., 2006). Each of these individual properties by themselves may not be indicative of fracturing with a high degree of certainty; however, when they are combined together into newly devised hybrid fracture zone identifier (FZI) attributes, they are postulated to provide reasonable indications of porous and fractured reservoir. It should be noted that we consider these as hybrid attributes because they use data from different sources (passive and reflection seismic as well as well logs). Although there could be many ways of designing such an attribute, we use a simple relationship defined as a nonlinear combination of input properties modeled using an ANN. The model can be represented as a function of normalized input attributes denoted by the subscript n:

$$\mathrm{FZI} = f(\phi_n, \rho_n, Z_{Pn}, V_{Sn}, V_{Pn}, V_{En}), \tag{1}$$

where ϕ_n is the porosity, ρ_n is the density, Z_{Pn} is the impedance, V_{Pn} and V_{Sn} indicate the P- and S-wave velocities, and V_{En} is the extensional velocity. These attributes were carefully selected from a broader set of attributes based on the least observed error when tested with data from the blind validation well. Porosity and density are effective properties derived from seismic and therefore should show clear variations in the presence of fractures. Velocities used are also critical because lower values indicate attenuation effects caused by open fluid-filled fractures. Some other attributes tested but not used for the final model include bulk modulus, Poisson's ratio, and tangential weakness (anisotropy) estimates. This was because they resulted in deterioration of validation results for corresponding models. This is most likely a result of available data quality and the fact that rock properties are likely harder to accurately predict compared to log properties because of available well constraints. Once the feature-scaled input attributes are available, training and validation data are extracted based on conductive and partially conductive fracture logs obtained from image log analysis.

Although the modeling for FZI can be carried out using different neural network modeling schemes, we use a simple multilayered normalized radial basis function neural network (RBFNN) as shown in Figure 11. Normalization allows for improved generalization of the network and provides for an excellent classifier:

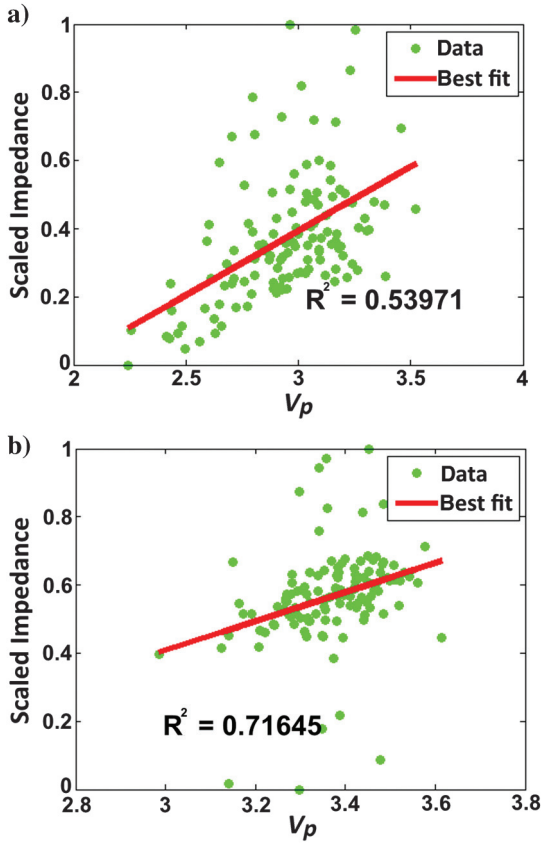

Figure 9. Scaled impedance correlated with compressional phase velocity with sampling points extracted from (a) $Z = 0.5$ km and (b) $Z = 1.0$ km. A relatively high correlation provides confidence in the use of impedance as the secondary constraint in cosimulation runs.

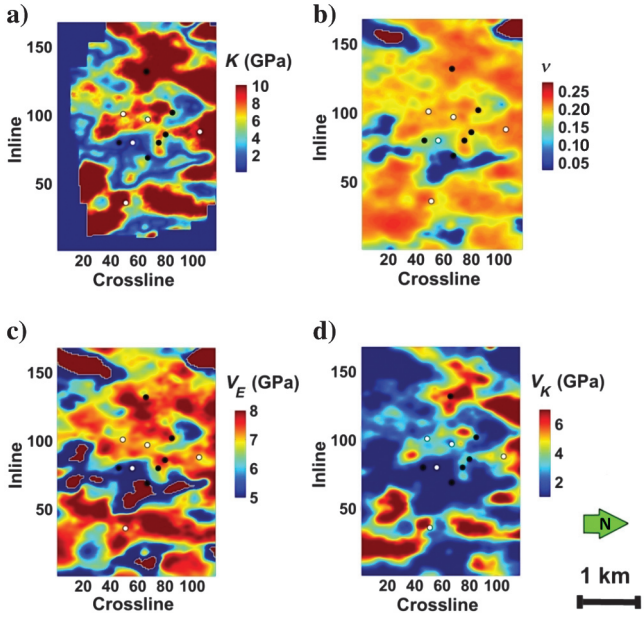

Figure 10. Depth slices at $Z = 1$ km through (a) bulk modulus, (b) Poisson's ratio, (c) extensional stress, and (d) hydrostatic stress volumes.

$$\varphi_i(x) = w_i e^{-(b\|x-x_i\|)^2}. \quad (2)$$

We use a Gaussian basis function with a bias "b" ensuring stability in evaluation and spread defining the selectivity of the functions. Here, ϕ_i defines the activation function at ith input node for input x, w_i is the associated weight of the node, and x_i represents the function centroid value. A sigmoid function is used at the output node to make sure that the results are range bound (between zero and one). It should be noted that there are other algorithms such as hybrid neurofuzzy or neuroevolutionary methods that can be used to obtain similar target-zone or fractured-zone identification properties including associated prediction uncertainties. An exhaustive look at various algorithms and a comparative study on which gives the best results has not been conducted because of the underlying data quality issues associated with available data. Figure 12 shows sample training data used in this study as well as training performance for the neural network before application of the trained model on the entire study volume.

Before evaluating the properties and making interpretations, zones showing very high uncertainties are trimmed based on simulation and inversion uncertain-

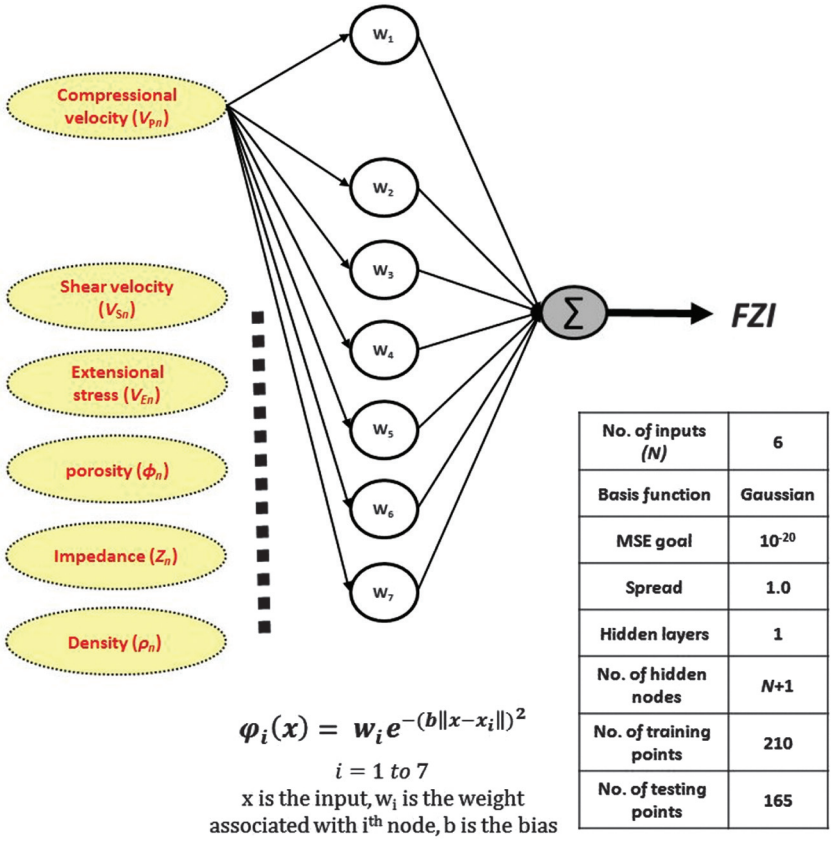

No. of inputs (N)	6
Basis function	Gaussian
MSE goal	10^{-20}
Spread	1.0
Hidden layers	1
No. of hidden nodes	N+1
No. of training points	210
No. of testing points	165

Figure 11. RBFNN design used for generating the FZI attribute. Inputs used (normalized phase velocities, extensional stress, porosity, impedance, and density) are derived from microseismic and seismic data analysis.

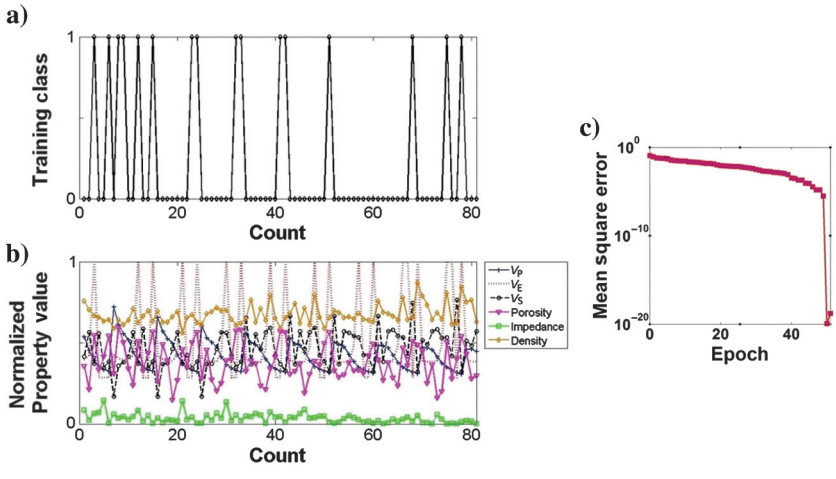

Figure 12. (a) Sample training data, (b) corresponding input properties, and (c) training results with RBFNN (supervised network design). The nodal inputs to the network include inverted wave velocities, extensional stress, porosity, impedance, and density volumes.

ties. Figure 13 shows the two evaluated uncertainty volumes for the same reference depth of 1 km. The final uncertainty is calculated by combining the normalized values from the simulation and inversion uncertainty estimates and the attribute is defined at locations where the uncertainty measure is low based on a threshold cutoff defined at the seventh quantile of the final uncertainty map. Figure 14 shows the distribution of the decimated FZI volume based on the cutoff with well inserts for reference. It should be noted that RBFNN is a characterization algorithm and the results show the probability of fractured zone presence through a classification value between zero and one.

Fracture zones from image log analysis not used for the neural network design are used to validate the final models. The inline and crossline projections shown in Figures 15 and 16 highlight the match obtained for the testing and validation case through the distribution of the FZI attribute at the well location. After the derived FZI model has been validated, we can use the attribute volume to identify other potential zones of interest that may hold prospects for future development or could help understand the reservoir behavior. It is important to note that the FZI attribute is qualitative and indicative

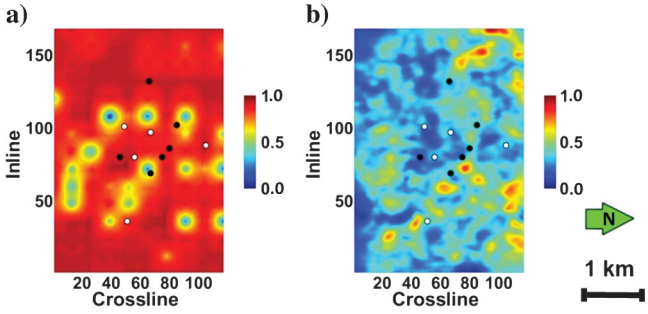

Figure 13. (a) Normalized tomographic inversion error and (b) normalized simulation error at reference depth (1 km) used to obtain uncertainties and to calculate property estimation cutoffs.

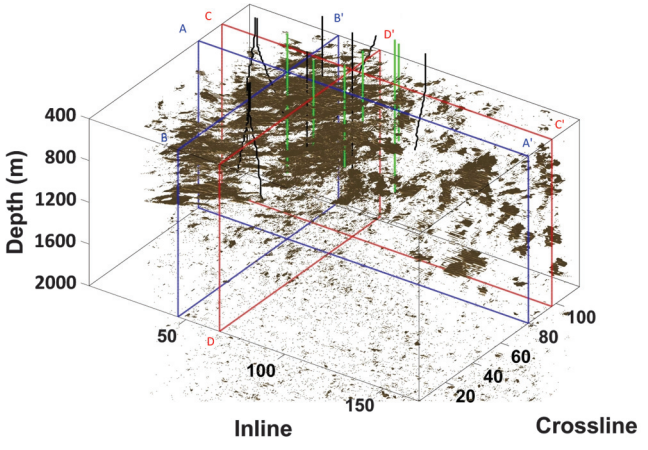

Figure 14. FZI attribute distribution in 3D with well locations. AA′ (BB′) shows the location of training well and CC′ (DD′) inserts show the location of the test well.

of potential fractured zones that could be of interest. It is necessary to validate the observations made by using other independent parameters such as the behavior of

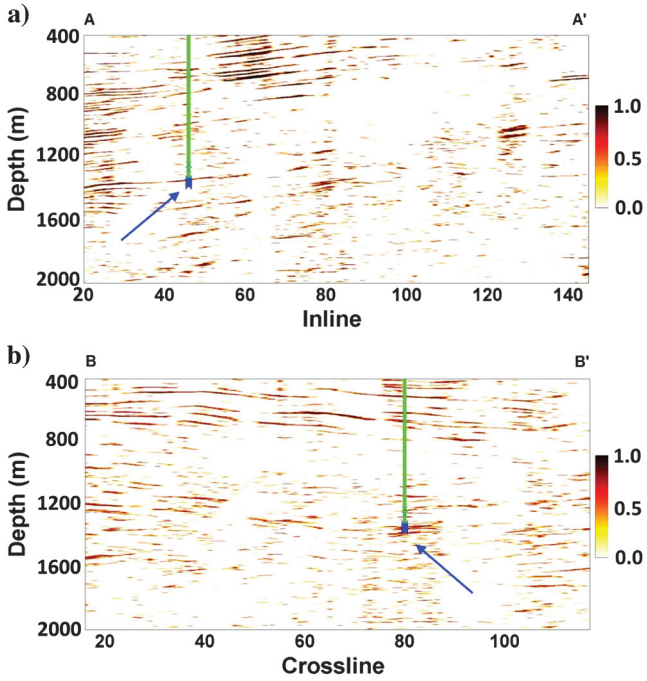

Figure 15. FZI attribute vertical slices along AA′ and BB′ through volume associated with the training well (data from logs used in ANN model design). Arrows indicate the location of high FZI values that match with known intervals showing fractures (blue inserts) over the green well tracks.

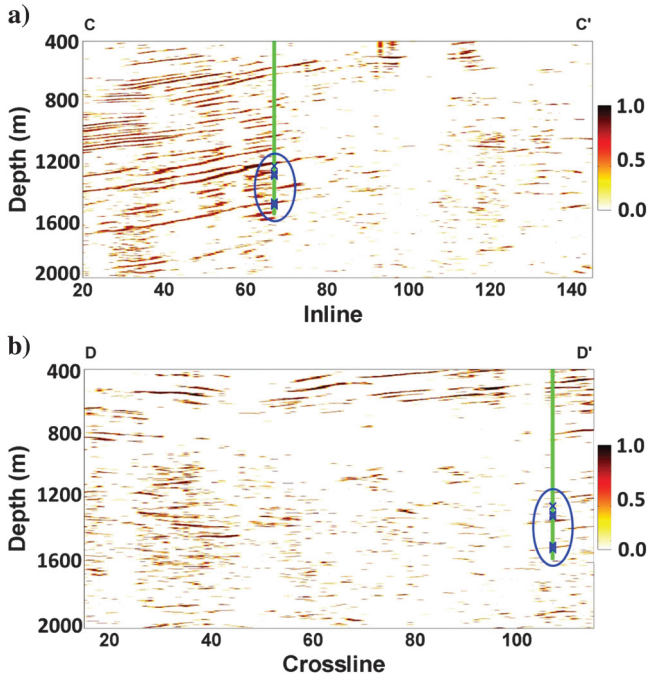

Figure 16. FZI attribute vertical slices along CC′ and DD′ through volume including the validation well with fractured zone interpreted from image logs. The projections show a high attribute value close to the fractured intervals (blue inserts) over the green well tracks.

other indicative properties and actual field data. We highlight the potential use of this attribute to better understand well behavior. Figure 17 shows small subsections from the FZI volume to highlight the distribution of the attribute close to four close wells of interest shown in Figure 17a. We observe from the evaluated property close to the wellbores that high FZI attributes show up at two depths of interest for three of the wells whereas for the fourth well, the lack of open fractures as interpreted through FZI attribute and the lack of major discontinuity close to the zone of interest could indicate the primary reason for low observed throughput for that producer. Similar analysis and interpretation can be carried out in zones away from the control wells. However, because many of the properties used in characterization are log derived, the confidence in the values at substantial distances from the wellbore are low and such interpretations could be prone to significant errors.

Because we have discussed of the potential for studying lateral connectivity, we carry out connectivity analysis by incorporating multiple properties concurrently in the same displays for specific depths of interest. In this case study, the producing zones were relatively shallow with significant unconsolidation because of loosely bound alluvial sediments created by the spreading zone and discontinuities because of an active geologic environment. This has created a major challenge in the picking of horizons due to the lack of spatial continuity. To address these issues, the maximized properties of greater than 10-m depth windows were used in subsequent integrated analysis. Figure 18 shows potential reservoir connectivity interpretations based on discontinuity from edge-enhanced or edge-preserved seismic attributes (contour map), the extensional stress gradient (arrow map), as well as the FZI attribute (variable density map). Figure 18a shows a sharp change in the stress gradient close to major discontinuity. We also observe high FZI values on both flanks of the discontinuity indicating potential contribution of fractured zone falling on the left flank of the discontinuity to the well productivity. The high FZI zone on the right flank could be contributing depending on the nature of the discontinuity, i.e., communicating or otherwise. Figure 18b shows high fracture probability only on one flank of the observed discontinuity close to the

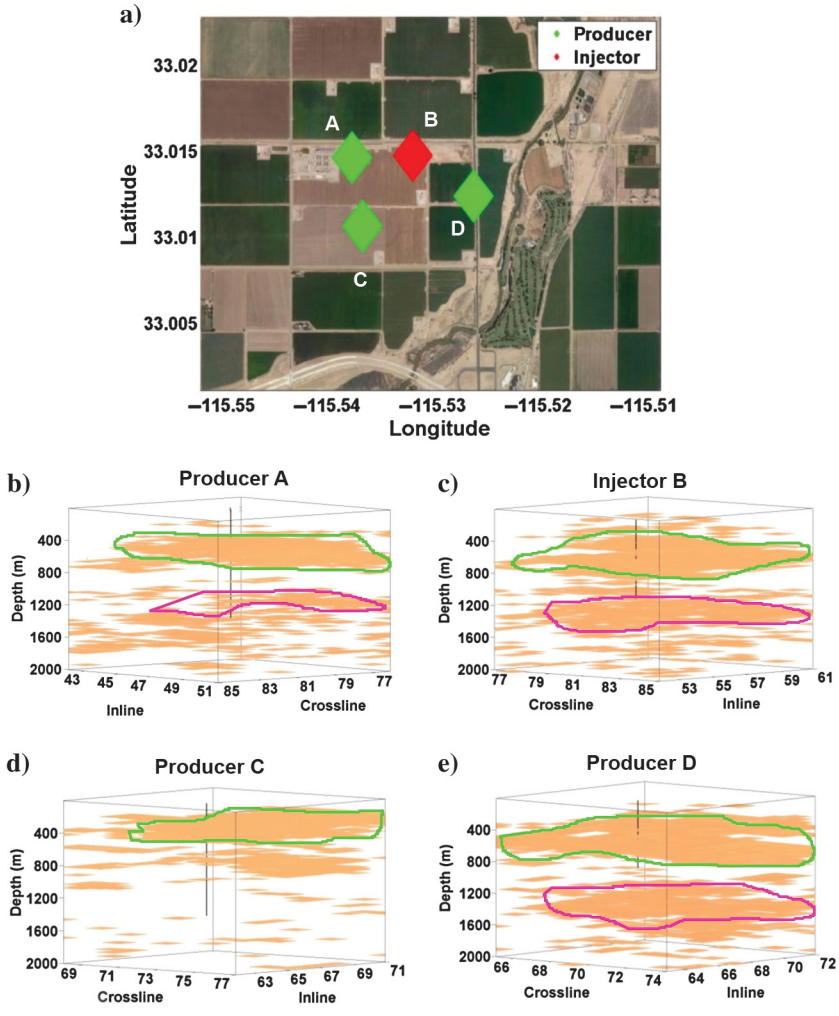

Figure 17. The near-wellbore distribution of the FZI attributes shown in (b) for producer A, (c) for injector B, (d) for producer C, and (e) for producer D with panel (a) showing the location of wells.

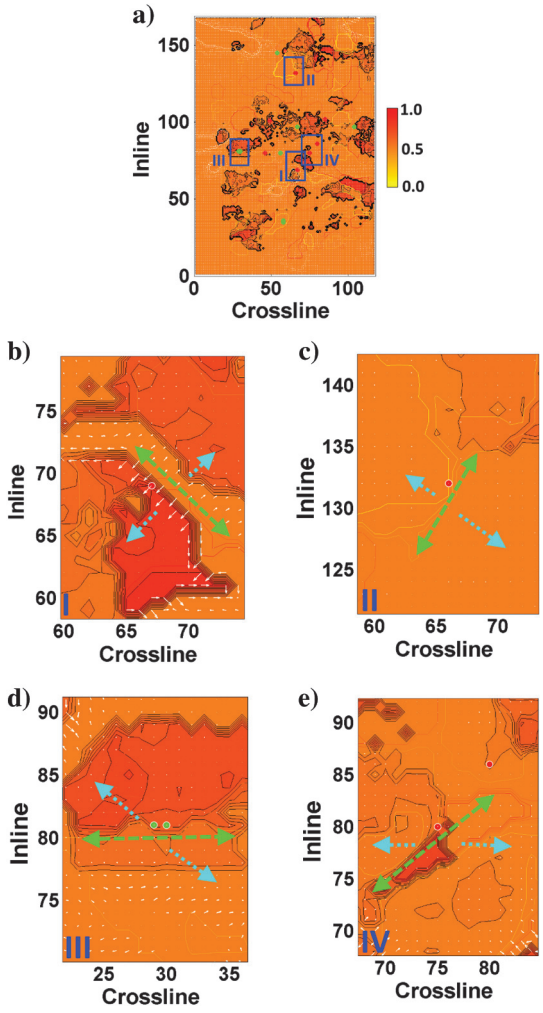

Figure 18. (a) Integrated (overlay) display at depth slice of $Z = 1$ km showing discontinuity (contour plot), FZI (variable density plot), and extensional stress gradient (vector plot) volumes close to production (red) and injection (green) wells. The blue inserts show the location of the four zones (b, c, d, and e). The green arrows indicate the discontinuity boundary, and the blue arrows indicate the change in the stress gradient close to the identified boundary.

wellbore of interest, and this could indicate the failure of injection wells to impact the other flank of the discontinuity, which could be because of fluid bypass or presence of noncommunicating fault. Figure 18c shows very low fracture probability close to the well of interest indicating flow dominated by discontinuities including major faulting close to the wellbore. Figure 18d shows highly fractured zone flanked by major discontinuity boundaries contributing to well productivity. We note that based on the simulation and inversion uncertainties, we expect all of our interpretations to hold because the said uncertainties are not very high at the four locations highlighted. However, among these four locations, location III shows the maximum mean uncertainty and therefore the corresponding interpretations can be prone to the most error.

Conclusions

Temporal analysis of microseismic data can help us understand the changes in the elastic properties with reservoir development. We have successfully demonstrated the potential for using microseismic data to generate usable rock property estimates, which in addition to seismic-derived properties can provide a framework for fracture-zone identification and characterization. This method can also be applied for other unconventional reservoir settings, and valuable information obtained from microseismic data can be of use to characterize the reservoir in question. Although we have developed a framework for fracture-zone identification, this method can easily be used for other types of characterization workflows including lithology, fluid type, fracture aperture, etc. Moreover, additional information such as fluid flow (based on flow models) and geologic models can also be integrated as additional constraints into the property models. The method also provides a framework for time-lapse fracture characterization for the field by potentially making use of temporally segmented catalogs. It is important to have a well-designed microseismic data acquisition scheme for useful application of the proposed workflow because the lack of adequate coverage and good-quality microseismic data place a major limitation on the final results obtained in this study. Such design issues and their impact on the final property volumes and interpretations will be looked into in the future.

Acknowledgments

This work was supported by Ormat, Inc., and we would like to acknowledge E. Zemach, S. Matlick, and P. Walsh for access to the data sets used in this study, for their valuable and timely inputs, and for permission to publish this work. For this study, we have used dGB's OpendTect software, open-source HypoDD and SimulPS packages, SGeMS geostatistical package, and MATLAB, and we would like to thank the respective authors for providing access to the relevant software. We also acknowledge contributions from Qiaosi Chen (USC).

References

Aminzadeh, F., 2003, Meta attributes: A new concept for reservoir characterization and seismic anomaly detection: Presented at 53rd Gulf Coast Association of Geological Societies Annual Convention.

Aminzadeh, F., 2005, A new concept for seismic anomaly detection: Presented at OTC, SPE.

Aminzadeh, F., and F. Brouwer, 2006, Integrating neural networks and fuzzy logic for improved reservoir property prediction and prospect ranking: 76th Annual International Meeting, SEG, Expanded Abstracts, 1752–1756.

Aminzadeh, F., and S. Chatterjee, 1984, Applications of cluster analysis in exploration seismology: Geoexploration; International Journal of Mining and Technical Geo-

physics and Related Subjects, **23**, 147–159, doi: 10.1016/0016-7142(84)90028-0.

Aminzadeh, F., and D. Connolly, 2002, Looking for gas chimneys and faults: AAPG Explorer, **23**, 20–21.

Aminzadeh, F., C. Ross, P. de Groot, and F. Brouwer, 2005, Hydrocarbon probability index based on ANN and pre-stack attributes: 67th Conference and Exhibition, EAGE, Extended Abstracts, F001.

Bakker, P., L. J. van Vliet, and P. W. Verbeek, 1999, Edge preserving orientation adaptive filtering: Proceedings of IEEE-CS Conference on Computer Vision and Pattern Recognition, IEEE Computer Society Press, 535–540.

Barnes, A. E., 2000, Weighted average seismic attributes: Geophysics, **65**, 275–285, doi: 10.1190/1.1444718.

Beer, F. P., E. R. Johnston, J. DeWolf, and D. Mazurek, 2009, Mechanics of materials: McGraw Hill.

Berge, P., L. Hutchings, J. Wagoner, and P. Kasameyer, 2001, Rock physics interpretation of P wave, Q and velocity structure, geology, fluids and fractures at the south east portion of the Geysers geothermal reservoir: GRC Transactions, **14**, 1–21.

Chopra, S., and K. J. Marfurt, 2007a, Seismic attributes for prospect identification and reservoir characterization: SEG.

Chopra, S., and K. J. Marfurt, 2007b, Volumetric curvature attributes for fault/fracture characterization: First Break, **25**, 35–46, doi: 10.3997/1365-2397.2007019.

Clifford, A., and F. Aminzadeh, 2011, Gas detection from absorption attributes and amplitude versus offset with artificial neural networks in Grand Bay Field: 81st Annual International Meeting, SEG, Expanded Abstracts, 375–380.

Crowell, J. C., and A. G. Sylvester, 1979, Tectonics of the juncture between the San Andreas fault system and the Salton Trough, southeastern California: A guidebook for fieldtrips: University of California, Santa Barbara.

Curtis, A., A. Michelini, D. Leslie, and A. Lomax, 2004, A deterministic algorithm for experimental design applied to tomographic and microseismic monitoring surveys: Geophysical Journal International, **157**, 595–606, doi: 10.1111/j.1365-246X.2004.02114.x.

Faust, L. Y., 1953, A velocity function including lithologic variation: Geophysics, **18**, 271–288, doi: 10.1190/1.1437869.

Gupta, N., S. Sarkar, and K. J. Marfurt, 2011, Seismic characterization of the Woodford shale in the Anadarko basin: 81st Annual International Meeting, SEG, Expanded Abstracts, 1083–1087.

Jahne, B., 1993, Digital image processing: Concepts, algorithms and scientific applications: Springer-Verlag.

Lancaster, S., and D. Whitcombe, 2000, Fast-track 'coloured' inversion: 70th Annual International Meeting, SEG, Expanded Abstracts, 1298–1301.

Lashgari, B., 1991, Fuzzy classification with application to geophysical data, *in* F. Aminzadeh, and M. A. Simaan, eds., Expert systems in exploration: SEG, 161–178.

Maity, D., 2013, Integrated reservoir characterization for unconventional reservoirs using seismic, microseismic and well log data: Ph.D. thesis, University of Southern California.

Maity, D., and F. Aminzadeh, 2012, Framework for time lapse fracture characterization using seismic, microseismic & well log data: 82nd Annual International Meeting, SEG, Expanded Abstracts, doi: 10.1190/segam2012-0387.1.

Maity, D., F. Aminzadeh, and M. Karrenbach, 2014, Novel hybrid artificial neural network based autopicking workflow for passive seismic data: Geophysical Prospecting, **62**, 834–847, doi: 10.1111/1365-2478.12125.

Maity, D., F. Aminzadeh, I. Salehi, and M. Karrenbach, 2013, Integrated approach toward multi-array microseismic survey design: 83rd Annual International Meeting, SEG, Expanded Abstracts, 2173–2177.

Martakis, N., S. Kapotas, and G. Tselentis, 2006, Integrated passive seismic acquisition and methodology: Case studies: Geophysical Prospecting, **54**, 829–847, doi: 10.1111/j.1365-2478.2006.00584.x.

Matlick, S., and T. Jayne, 2008, Brawley — Resurrection of a previously developed geothermal field: GRC Transactions, **32**, 159–162.

Mavko, G., T. Mukherji, and J. Dvorkin, 2003, The rock physics handbook: Cambridge University Press.

Remy, N., A. Boucher, and J. Wu, 2009, Applied geostatistics with SGeMS: Cambridge University Press.

Rudman, A. J., J. F. Whaley, R. F. Blakely, and M. E. Biggs, 1976, Transformation of resistivity to pseudo velocity logs: AAPG Bulletin, **59**, 1151–1165.

Russell, B., D. Hampson, J. Schuelke, and J. Quirein, 1997, Multiattribute seismic analysis: The Leading Edge, **16**, 1439–1444, doi: 10.1190/1.1437486.

SCEDC (2013): Southern California earthquake center: Caltech. Dataset, doi:10.7909/C3WD3xH1.

Schuelke, J. S., and J. A. Quirein, 1998, Validation: A technique for selecting seismic attributes and verifying results: 68th Annual International Meeting, SEG, Expanded Abstracts, 936–939.

Taner, M. T., F. Koehler, and R. E. Sheriff, 1979, Complex seismic trace analysis: Geophysics, **44**, 1041–1063, doi: 10.1190/1.1440994.

Thurber, C. H., 1993, Local earthquake tomography: Velocities and V_P/V_S — theory, *in* H. M. Iyer, and K. Hirahara, eds., Seismic tomography — Theory and practice: Chapman & Hall, 563–583.

Toksöz, M. N., and D. H. Johnston, 1981, Seismic wave attenuation: SEG.

Trinchero, E., L. Vernengo, and J. Cardoso, 2013, Geomechanical and geometric seismic attributes in an interpretation workflow for characterization of unconventional reservoirs: The Leading Edge, **32**, 386–392, doi: 10.1190/tle32040386.1.

Waldhauser, F., and W. L. Ellsworth, 2000, A double-difference earthquake location algorithm: Method and appli-

cation to the northern Hayward fault: Bulletin of the Seismological Society of America, **90**, 1353–1368, doi: 10.1785/0120000006.

Walls, J. D., M. T. Taner, T. Guidish, G. Taylor, D. Dumas, and N. Derzhi, 1999, North Sea reservoir characterization using rock physics, seismic attributes, and neural networks: A case history: 69th Annual International Meeting, SEG, Expanded Abstracts, 1572–1575.

Debotyam Maity received M.S. and Ph.D. (2013) degrees from the University of Southern California (USC). Since 2013, he has been working with the Gas Technology Institute as a principal engineer. His main research interests include reservoir characterization, passive seismic data processing and analysis, and well completion design and diagnostics with a particular focus on unconventional oil and gas reservoirs.

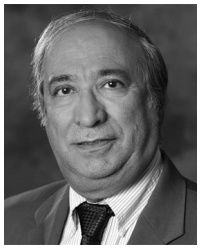

Fred Aminzadeh is a research professor at USC. He is also the director of Global Energy Network, Induced Seismicity Consortium and Reservoir Monitoring Consortium at USC. He served as president of SEG in 2007–2008. Before joining USC, he was the president and CEO of dGB Earth Sciences USA and previously worked for Unocal in technical and management positions. He is a fellow of IEEE, a member of the Russian Academy of Sciences, a member of the Azerbaijan Oil Academy, and the National Research Council's Committee on Seismology. He has served as a member of DOE's Unconventional Resources Technology Advisory Committee, as the chairman of the SEG Research Committee, and has received many awards including SEG's Commendation Award (2005) and the SPE Western North American Region Award for Reservoir Description and Analysis (2011).